Journal of Materials Chemistry C

Accepted Manuscript

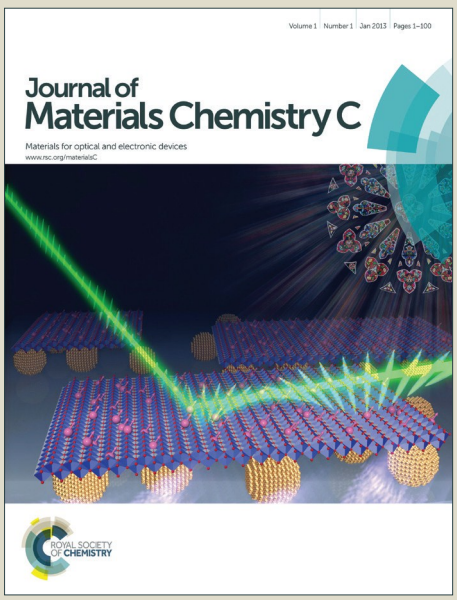

ROYAL SOCIETY OF CHEMISTRY

www.rsc.org/materialsC

Emission Stability and Reversibility of Upconversion Nanocrystals

Deming Liu[1,2,3], Xiaoxue Xu[1,2,3,*], Fan Wang[1,2,3], Jiajia Zhou[3,4], Chao Mi[2,3], Lixin Zhang[1], Yiqing Lu[1], Chenshuo Ma[1], Ewa Goldys[1], Jun Lin[3,5], and Dayong Jin[1,2,3,*]

[1] Advanced Cytometry Labs, ARC Centre of Excellence for Nanoscale BioPhotonics, Macquarie University, Sydney, NSW, 2109, Australia;

[2] Institute for Biomedical Materials and Devices, Faculty of Science, University of Technology Sydney, NSW, 2007, Australia;

[3] Australian Research Council Research Hub for Integrated Device for End-user Analysis at Low-levels (IDEAL), Faculty of Science, University of Technology Sydney, NSW, 2007, Australia;

[4] College of Optical Science and Engineering, State Key Laboratory of Modern Optical Instrumentation, Zhejiang University, Hangzhou, 310027, P. R. China;

[5] State Key Laboratory of Rare Earth Resource Utilization, Changchun Institute of Applied Chemistry, Chinese Academy of Sciences, Changchun, 130022, P. R. China.

[*] *Email: xiaoxue.xu@mq.edu.au; dayong.jin@uts.edu.au*

Abstract:

Rare-earth doped upconversion nanocrystals have emerged as a novel class of luminescent probes for biomedical applications. The knowledge about their optical stability in aqueous solution at different pH and temperature conditions has not been comprehensively explored. Here we conduct a systematic investigation and report the emission stability and reversibility of the typical $NaYF_4$: Yb^{3+},Er^{3+} nanocrystals and their core-shell nanostructures in aqueous solution at different temperatures and with different pH values. These nanocrystals show reversible luminescence response to temperature changes, while low pH permanently quenches their luminescence. With the addition of inert shells, with thickness ranging from 1.5 nm to 8 nm, the emission stability and reversibility change significantly. Thicker inert shells not only lead to significant enhancement in the emission intensity but also stabilize its optical responses which becomes less affected by temperature variations and pH conditions. This study suggests that upconversion nanocrystal-based sensitive temperature and pH sensors do not generally benefit from the core-shell structure usually recommended for enhanced upconversion luminescence.

Introduction

Lanthanide-doped upconversion nanoparticles (UCNPs) that absorb near infrared excitation and exhibit anti-Stokes emission in visible and ultra-violet have attracted significant interest in the last decade[1, 2]. They offer key advantages in bioimaging and luminescence detection including low detection background, tunable emission spectrum [3] and decay lifetime [4, 5], absence of photo-bleaching and blinking [6, 7], deep penetration of the excitation exciting light [8], and low toxicity with excellent chemical and biological compatibility[9, 10]. They are widely regarded as ideal luminescent probes for a range of biomedical applications, such as ultrasensitive biomolecular assays [11-14], multimodal biomedical imaging [15-21], and photodynamic therapies[22, 23].

Several groups reported that UCNPs can serve as accurate nanoscale sensors for intracellular monitoring of temperature [24] or pH [25]. They can also be applied as photo responsive carriers for controlled delivery and release of drugs *in vivo* [26-31], where high temperature and/or lower pH conditions trigger drug release. The ratio-metric green emissions of Er^{3+} doped UCNPs are sensitive to cellular temperature with a resolution of 0.5 °C in biological range of 25 °C to 45 °C[32]. The red emission of the Er^{3+} UCNPs was found to be responsive to pH variations and to increase at low pH.[32] Li and co-workers recently reported a hybrid design of carbon@ inert shell @UCNPs for real-time monitoring of the localized temperature increase during photodynamic therapy.[33] We demonstrated a drug release sensing scheme by using the luminescence intensity of UCNPs. In this scheme we monitored the drug release process in the low pH environment (around pH=5), as the drug on the surface of UCNPs was designed to quench the luminescence increasing upon drug release [34].

The understanding of luminescence responses to the varied temperature and pH environment[35-37] require more detailed consideration of the stability and reversibility of UCNPs luminescence in different pH and temperature conditions. The literature reports on the subject remain divided. Wei et al. reported stable emission of the UC nanocrystals with different surface ligands, but it was only tested at neutral pH in aqueous solutions [38]. Li et al. reported thermal stability of UCNPs and an anomalous relationship between temperature and the upconversion luminescence.[39, 40] Xu et al. reported α–$NaYb(Mn)F_4:Er^{3+}$@$NaYF_4$ UCNPs can be applied as luminescent nano-thermometers over a wide temperature range. But these tests were done only for the dry powder.

Coating inert shells onto the core UCNPs is a well-established and effective solution to minimize the surface quenching effect and therefore to enhance the upconversion luminescence by a factor of several to

hundreds, depending on core size and shell thickness. [41-44] However, the role of the inert shells in influencing the stability and reversibility of luminescence at varied pH and temperature in aqueous solution has not yet been investigated.

In this work, we systematically investigated and compared the luminescence response of Er^{3+} doped UCNPs to different pH and temperature in aqueous solution for both core-only and core-shell UCNPs. Using a modified hot-injection method, we prepared a systematic series of UCNPs by epitaxial growth of the homogeneous $NaYF_4$:Yb^{3+}, Er^{3+} UCNPs with different shell thicknesses from 1.5 to 8 nm. To characterize these nanoparticles in aqueous solution, we removed the surface organic ligands oleic acids and transfer the hydrophilic UCNPs into the aqueous phase using an acid-based ligand removal method reported by Capobianco et al. [45] We chose this approach to reduce the influence of surface ligands [38] on UCNP upconversion luminescence. Our results show that the luminescence intensity of UCNPs decreases in either acid or alkali pH environment. In acidic environment this luminescence decrease is not reversible. Conversely, higher temperature significantly reduces the luminescence intensity in a reversible way. The inert shell also reduces the sensitivity and resolution of the ratio-metric response of green emissions (524 nm/ 545 nm) of Er^{3+} doped UCNPs for temperature sensing below 60 ^{o}C. This work compliments the current knowledge underpinning the rapid development of upconversion nanosensors for emerging biomedical applications and further suggests that new careful designs are necessary to accurately sense temperature and pH in specific applications.

Materials and Methods:

Yttrium chloride hexahydrate ($YCl_3 \cdot 6H_2O$, 99.99%), ytterbium chloride hexahydrate ($YbCl_3 \cdot 6H_2O$, 99.998%), erbium chloride hexahydrate ($ErCl_3 \cdot 6H_2O$, 99.9%), sodium hydroxide (NaOH, 98%), ammonium fluoride (NH_4F, 99.99%), oleic acid (OA, 90%), 1-octadecene (ODE, 90%) and hydrochloric acid (HCl, 37%) were purchased from Sigma-Aldrich. Oleylamine (OM, 90%) was purchased from Pfaltz & Bauer. All reagents were used as received without further purification.

Synthesis of β-$NaYF_4$:Yb^{3+},Er^{3+} cores

A modified synthesis method was adopted to prepare β-$NaYF_4$:20%Yb^{3+}, 2%Er^{3+} as core UCNPs. In a typical procedure, 1 mL of $LnCl_3$ in methanol (1.0 mmol, Ln=Y, Yb, Er) was mixed with OA (6 mL) and ODE 15 mL) in a 100 mL three-neck round-bottom flask. The mixture solution was degassed under Ar flow during the heating up to 150 °C followed by 30 min isothermal reaction to form a clear solution, and then cooled down to room temperature. 10 mL of methanol containing NH_4F (4 mmol) and NaOH (2.5 mmol) was added into the

flask and then stirred for 60 min. The solution was slowly heated up to 110 °C and kept at 110 °C for 30 min to completely remove the methanol and any residual water. Then the reaction solution was quickly heated up to 310 °C and kept isothermally for 1 h, before cooled down to room temperature. Ethanol was added to precipitate the nanocrystals, which were washed 4 times with cyclohexane, ethanol and methanol. The obtained pure $NaYF_4$:Yb^{3+},Er^{3+} nanocrystals were re-dispersed in 10 mL of cyclohexane for coating inert shell.

Synthesis of α-$NaYF_4$ shell precursors

A modified literature method [46] was used, with all the preparation and pre-treatment steps similar as in the $NaYF_4$ cores synthesis method. The only two differences were that lanthanide precursor was changed to be 1 mmol YCl_3 and the reaction temperature became 290 °C (instead of 310 °C). After the reaction, the nanoparticles were washed and re-dispersed in cyclohexane. The obtained pure α-$NaYF_4$ seeds in cyclohexane solution was mixed with 10 ml ODE in one 100 ml three-neck flask. Then, the mixture was kept at 110 °C for 30 min under Ar flow. After the mixture was cooled to room temperature, α-$NaYF_4$ ODE solution as the precursor of the inert shell was obtained.

Synthesis of β-$NaYF_4$:Yb^{3+},Er^{3+}@$NaYF_4$ core-shell nanocrystals

A modified hot-injection method [46] was used for growing undoped shells onto the core nanocrystals. 1 mL (0.2 mmol Ln^{3+}) of obtained α-$NaYF_4$:Yb^{3+},Er^{3+} cyclohexane stock solution was mixed with OA (5 mL), OM (1 mL) and ODE (8 mL) in a 100 mL three-neck flask. The mixture was degassed under Ar flow and kept at 110 ^{o}C for 30 min to completely remove cyclohexane as well as any residual water. After that, it was quickly heated to 305 ^{o}C and the pure α-$NaYF_4$ seeds in ODE solution was injected using syringe (injection rate 0.05 mmol α-$NaYF_4$ seeds solution every 10 min; total amounts injected α-$NaYF_4$ seeds for different thickness shell refer to Supplementary Table 1). After the reaction, the precipitate was washed and stored in cyclohexane.

Characterizations

Standard transmission electron microscope (TEM) measurements were performed using a Philips CM10 TEM with Olympus Sis Megaview G2 Digital Camera. The samples were prepared for TEM analysis by placing a drop of a dilute suspension of nanocrystals onto formvar-coated copper grids (300 meshes) and were allowed to dry in a desiccator at room temperature before using. Powder X-ray diffraction (XRD) patterns were obtained on a PANalytical X'Pert Pro MPD X-ray diffractometer using Cu Kα1 radiation (40 kV, 40 mA, λ=0.15418 nm). The XRD samples were prepared by repeatedly drying drops of nanocrystal dispersions in cyclohexane cast on a zero-background silicon wafer. The temperature-dependent and pH dependent upconversion

luminescence spectra of colloidal solutions in quartz cuvettes with 10 mm path length were acquired with a Fluorolog-Tau3 spectrofluorometer (JobinYvon-Horiba) equipped with an external 980 nm CW diode laser with a pump power of 200 mW. UCNPs in the aqueous dispersion were tuned to own the same number concentration. Temperature control is via a homemade water bath equipment.The pH values of UCNPs dispersed in aqueous solution were adjusted with Milli-Q water, pH=3 of PBS solution and pH=12 of PBS solution. The luminescence lifetimes were measured by a purpose-built high-throughput 3-dimentional time-resolved spectroscopy[47], with pulsed 980 nm laser excitation (100 mW) at a repetition rate of 50 Hz.

Results and discussion

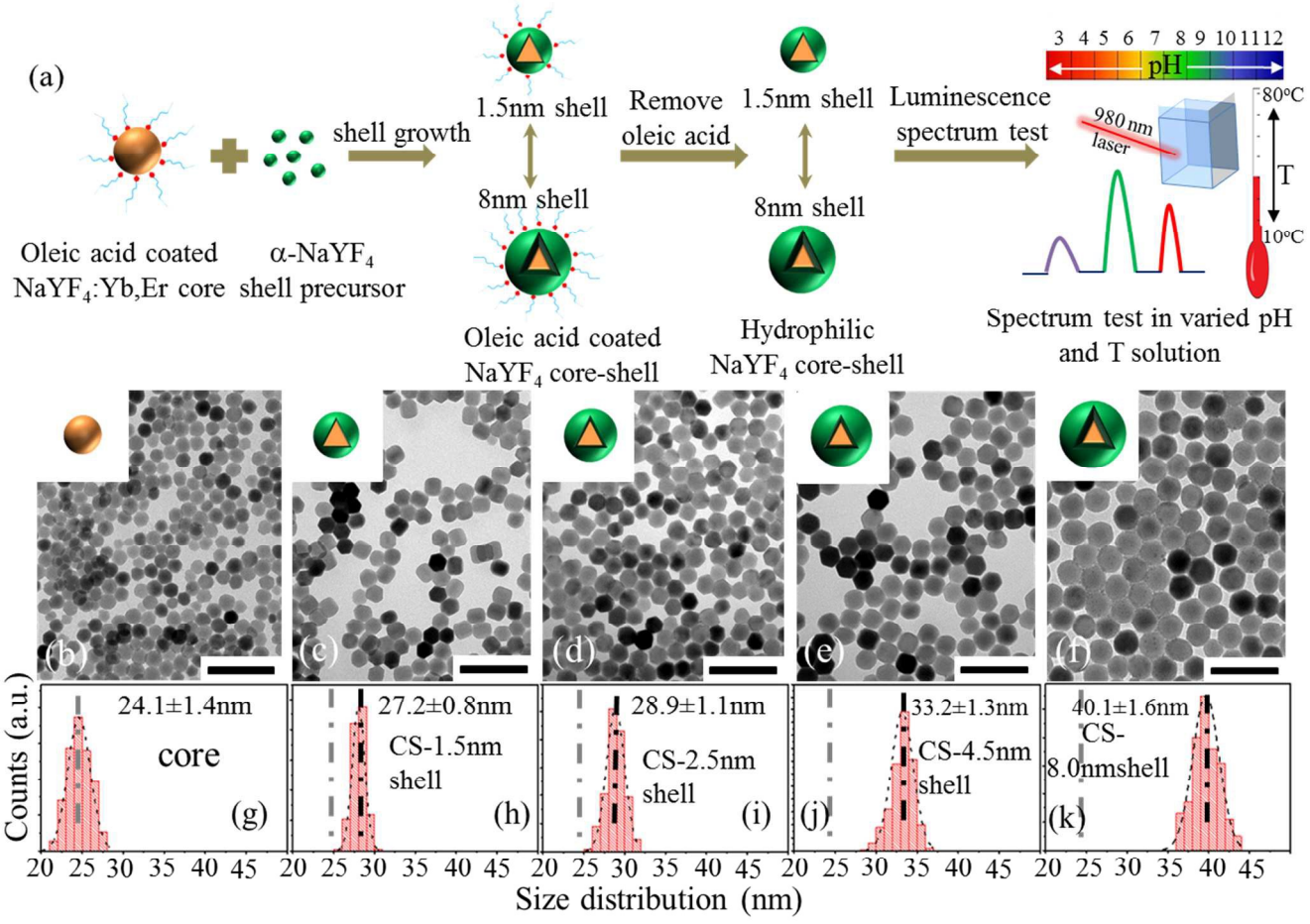

Figure 1 Synthesis and testing the core and core-shell UCNPs' luminescence response to varied pH and temperature environment (a), TEM images and size distribution charts of core-only (b,g) and core-shell UCNPs with 1.5 nm (c, h), 2.5 nm (d, i), 4.5 nm (e, j) and 8.0 nm (f, k) homogeneous $NaYF_4$ shell. (Scale bar: 50 nm)

Figure 1 illustrates our design of the experiments to systematically study the luminescence response of core-shell UCNPs in aqueous solution at varied pH and temperature environment. Homogeneous core-shell

structure were synthesized on the $NaYF_4$:Yb^{3+},Er^{3+} core UCNPs by controlling the amount of OM in a hot injection method (supplementary Figure S1). The shell thickness of homogeneous core-shell UCNPs was controlled by adjusting the amount of shell precursors. (supplementary Table S1). Figure S2 showed that the 24 nm β- $NaYF_4$:Yb^{3+},Er^{3+} core was sequentially coated with a series of different thickness $NaYF_4$ shells. These samples were treated by a diluted acid solution to remove the surface ligands so that the as-prepared UCNPs became hydrophilic and were transferred into aqueous solution (Figure 1 a). Such ligand-free UCNPs will avoid the test influence from surface ligands. Figure 1 b-k shows the morphology characterizations of the as-prepared hydrophilic core and core-shell UCNP samples. $NaYF_4$: Yb^{3+},Er^{3+} core UCNPs displayed uniform spherical shape, with average size of 24.1 nm (Figure 1 b & g) and a narrow size distribution. The core-shell nanocrystals were also spherical, with average size of 27.2 nm, 28.9 nm, 33.2 nm and 40.2 nm, respectively, and a narrow size distributions at (Figure 1 c-f). Their average shell thickness was calculated by comparing the average diameters of core and core-shell nanocrystals from Figure 1 (g-k). [48]

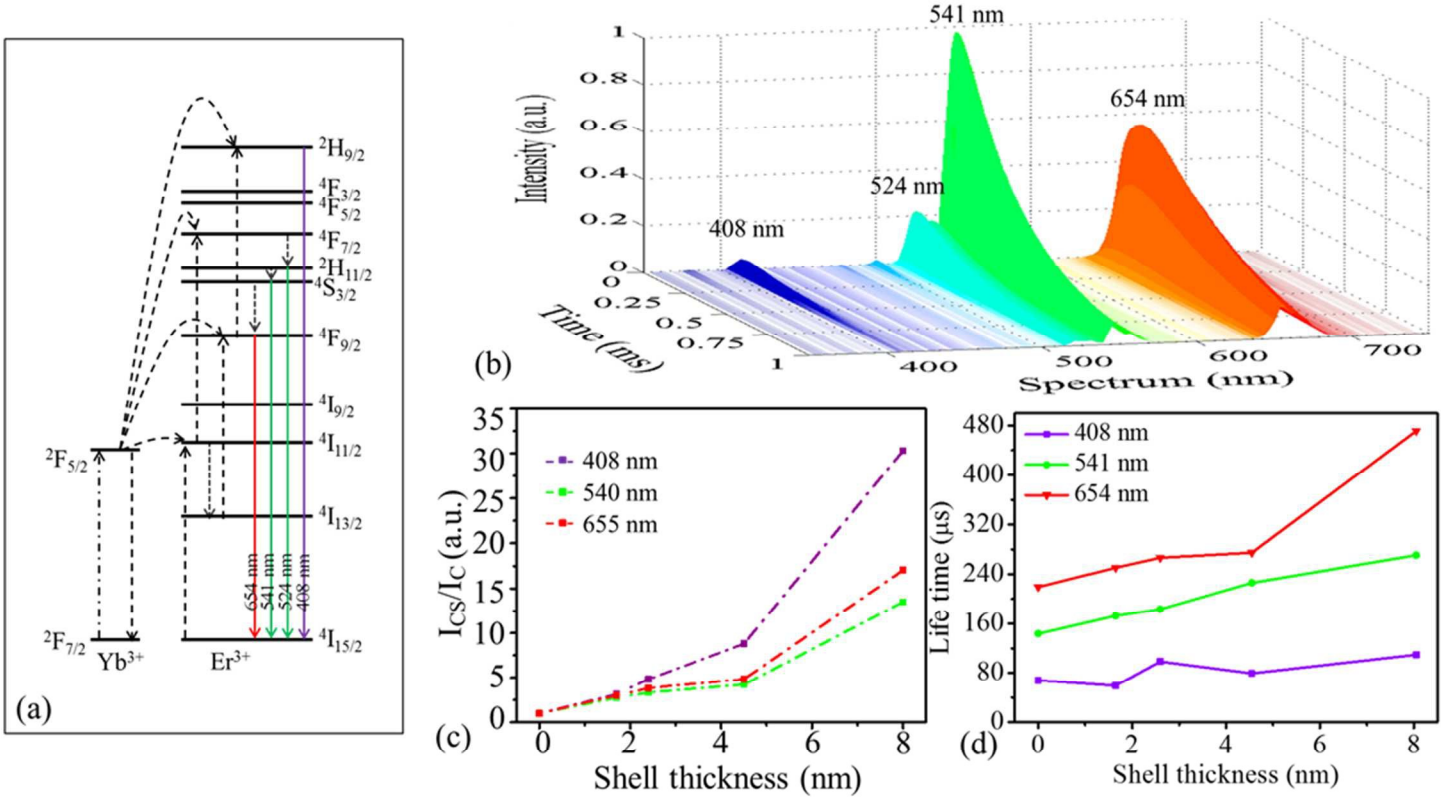

Figure 2 (a) Schematic illustration of the transition energy levels of $NaYF_4$: Yb^{3+},Er^{3+} nanocrystals. Arrows Indicate: ⇢ NIR excitation, ⇢ energy transfers, ⇢ multiphonon nonradiative relaxation, → , → , → upconversion emissions (b) Typical real-time resolved emission spectrum of $NaYF_4$: Yb^{3+},Er^{3+} UCNPs. Intensity enhancement factors (c) and luminescence decay lifetimes (d) for emissions at 408 nm, 540 nm and 655 nm were plotted as functions of shell thickness.

Figure 2 (a) illustrates the major four emissions' energy transfer processes between energy levels of Yb^{3+} and Er^{3+} under 980 nm light excitation. The three-dimensional time resolved luminescence spectrum of UCNPs was obtained by a high-throughput time-resolved luminescence spectroscopy that simultaneously provides the emission spectrum and lifetime decay curve, as shown in Figure 2 (b). The luminescence enhancement and increased lifetimes due to coating the UCNPs with the inert shells (as shown in supplementary Figure S3 and S4) was consistent with other reports in the literature[43, 46, 49-51]. Figure 2(c) shows that the enhancement of emissions increased with increased thickness of the shells, while enhancement factors at varied emission positions were also different. The emission peaks at 408 nm, 540 nm, and 655 nm were only enhanced by about 3 times by coating a 1.5 nm inert $NaYF_4$ shell, and the enhancement factors of 30, 12 and 15 were achieved for these peaks when a 8 nm shell was coated. Similar exceptional enhancement of violet emissions was also observed for the $NaYF_4$:Yb^{3+}, Tm^{3+}@CaF_2 core-shell nanocrystals.[52] This suggested that higher order energy transfer processes benefited more from the inert shell protection. The luminescence lifetime data, shown in Figure 2 (d), further confirmed that the uniform shells coated onto the core UCNPs. The luminescence lifetimes from the three emission bands (violet, green and red) increased with thicker shells. Both these strongly enhanced emission intensities and significantly longer lifetimes confirmed our successful growth of a series of homogeneous core-shell UCNPs.

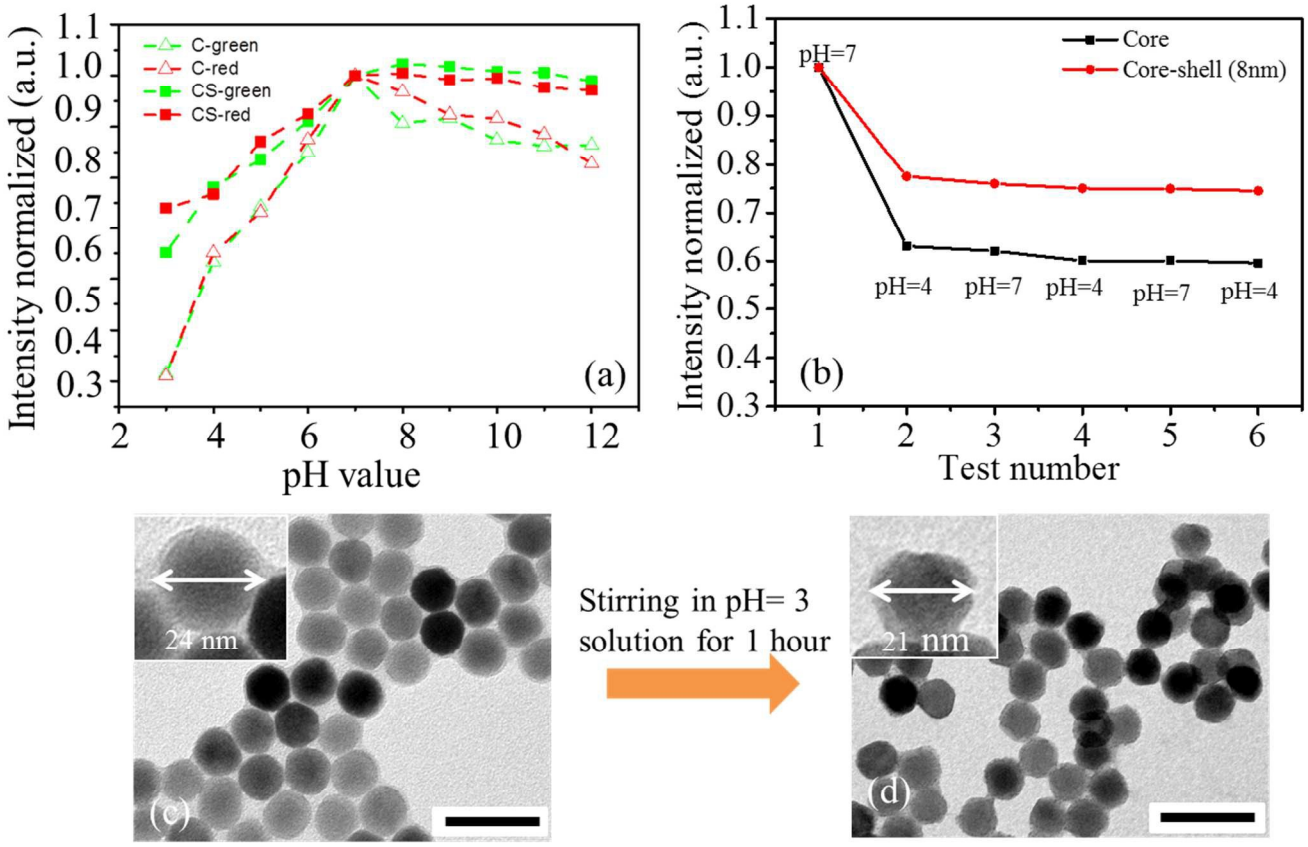

Figure 3 (a) Luminescence responses of the $NaYF_4$: Yb^{3+}, Er^{3+}core UCNPs and $NaYF_4$: Yb^{3+}, Er^{3+} @$NaYF_4$ core-shell UCNPs in the green (524 nm and 545 nm) and red emission bands. The data was normalized at pH=7 and plotted as function of pH values of the solution. (b) The reversibility test for the 655 nm emissions of the core and core-shell UCNPs by switching the pH values between pH=4 and pH=7. TEM images of ligand free UCNPs before (c) and after (d) stirring in pH=3 solution for 1 hour. (Scale bar is 50 nm)

Figure 3 and Figure S5 show the impact of the shell on the luminescence stability and reversibility against pH changes. The luminescence spectra of core-only and core-shell UCNPs were tested in aqueous solution under varied pH. Figure S5 shows that the acidic solution had a strong quenching effect on the UCNPs' luminescence and the inert shells were able to alleviate the quenching to some degree. Both the green and red emissions displayed similar emission quenching trends with the pH decreasing (Figure 3 (a)). The green emission from the core UCNPs decreased to 28% of its initial intensity with pH decreasing from 7 to 3, while the green emission from the core-shell UCNPs only decreased to about 65% of its original intensity. The alkaline conditions have been found to have less influence on the emissions. The emission from the core UCNPs was reduced only by 20% with pH increasing from 7 to 12, while the emission from core-shell UCNPs

only experienced a slight decrease in alkaline conditions. These data showed the inert shells help to improve the luminescence stability against pH changes.

Figure 3 (b) shows luminescence reversibility of luminescence of the core and core-shell UCNPs when repeatedly varying the pH conditions between pH=4 and pH=7. The quenching effect by the acidic aqueous solution was not reversible regardless of the presence of thick inert shells. Once the pH of the samples was decreased to pH=4 for less than ten minutes, irreversible luminescence quenching occurred. Luminescence in these samples did not recovered even by bringing the pH back to 7. The irreversible luminescence quenching of the UNCPs in the acidic environment suggested that the crystal surface may experience chemical damage at the low pH conditions.. To prove this, we carefully compared the TEM images of ligand free UCNPs before (Figure 3(c)) and after (Figure 3 (d)) the pH=3 acid solution treatment for 1 hour. Interestingly, we observed an obvious reduce in size from 24 nm to 21 nm and a rough surface morphology, showing that the nanocrystals were chemically etched. These chemical damage from weak acid was also found in other rare earth fluorides nanocrystals, such as $NaEuF_4$,[53] and $Lu_6O_5F_8$ [54]. We attributed this to the dissociation of Ln-F bonds of the $NaYF_4$ nanocrystals in the solution with low pH (≤ 3).

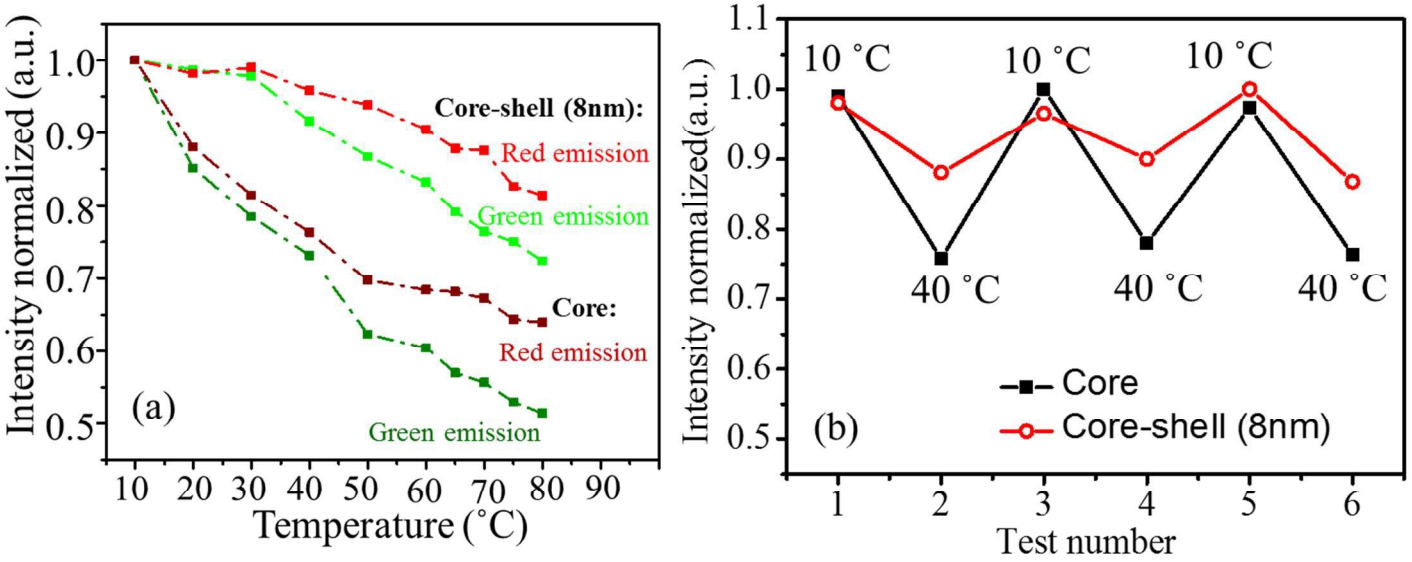

Figure 4 (a) The intensity response at green and red bands for the core and core-shell UCNPs as function of temperature. The data was normalized at 10 ˚C; (b) Green emission intensity response as function of temperature repeatedly switched between 10 ˚C and 40 ˚C.

We further measured the spectra of $NaYF_4:Yb^{3+}$, Er^{3+} core-only and core-shell UCNPs in Milli-Q water at varied temperatures from 10 ˚C to 80 ˚C (shown in Figure 4 and Figure S6). Figure S6 (a - b) shows the

luminescence intensities of both core-only and core-shell nanocrystals decreased at higher temperature with the core UCNPs being more strongly affected. The green emission of the core-only UCNPs decreased quickly to 78% of its original intensity even the temperature was only raised from 10 ˚C to 30˚C. With further temperature increase from 30 ˚C to 80 ˚C, the green emission decreased to nearly half of its original intensity at 10 ^{o}C. The shell protection again was found to alleviate the temperature-induced quenching, with the green emission from the core-shell UCNPs decreasing by only 27% at 80 ˚C. The quenching of the red emission was similar to the green emission, when it occurred at lower temperatures from 10 ˚C to 40 ˚C). However, the red emission has slightly higher stability than the green emission at higher temperature range from 40 ˚C to 80 ˚C. We think that the reason of red emission receiving lower quenching effect than the green emission at the higher temperature range is due to an increase of population transition from at $^{4}S_{3/2}$ to $^{4}F_{9/2}$. According to Xiaogang Liu group's investigation [55] on the relationship between relative emission intensity and nanocrystal surface defects that the higher energy level excited state would receive multiphonon nonradioactive relax from surface quenchers. The relative low energy level of $^{4}F_{9/2}$ would receive some population from the higher energy levels (e.g. $^{4}S_{3/2}$), therefore the red emission presents relative higher stability than the green emission at higher temperature.

Figure 4(b) demonstrates the reversibility of the luminescence emission against temperature, and it shows that the emission intensities of both the core-only and core-shell nanocrystals followed the temperature change between 10 ˚C and 40 ˚C, and these changes were fully reversible. The degree of intensity variations for the core-shell nanocrystals was lower than that of the core nanocrystals. These results suggested that the core-shell structure of $NaYF_4$:Yb^{3+}, Er^{3+} /$NaYF_4$ has a less pronounced response to temperature variations, especially in the range from 10 ˚C to 40 ˚C, relevant for *in vivo* biomedical applications. The observed improvement on emission stability by coating the passivation shell suggested that the inert shell can effectively reduce quenching effect from the vibrational energies and optical traps arising from particle surface. The water molecule is known as a surface oscillator that significantly quenches the luminescence of lanthanide dopant ions, because of the high energy (ca. 3500 cm^{-1}) of the stretching vibration. As the temperature rising, the water molecular on the crystal surface could be more intensely vibrating, which may affect the Ln-F bond on the crystal surface and create more phonons. Coating inert shell structure, forming a gap between the emitters and the quenchers can effectively reduce the quenching effect caused by temperature rising.

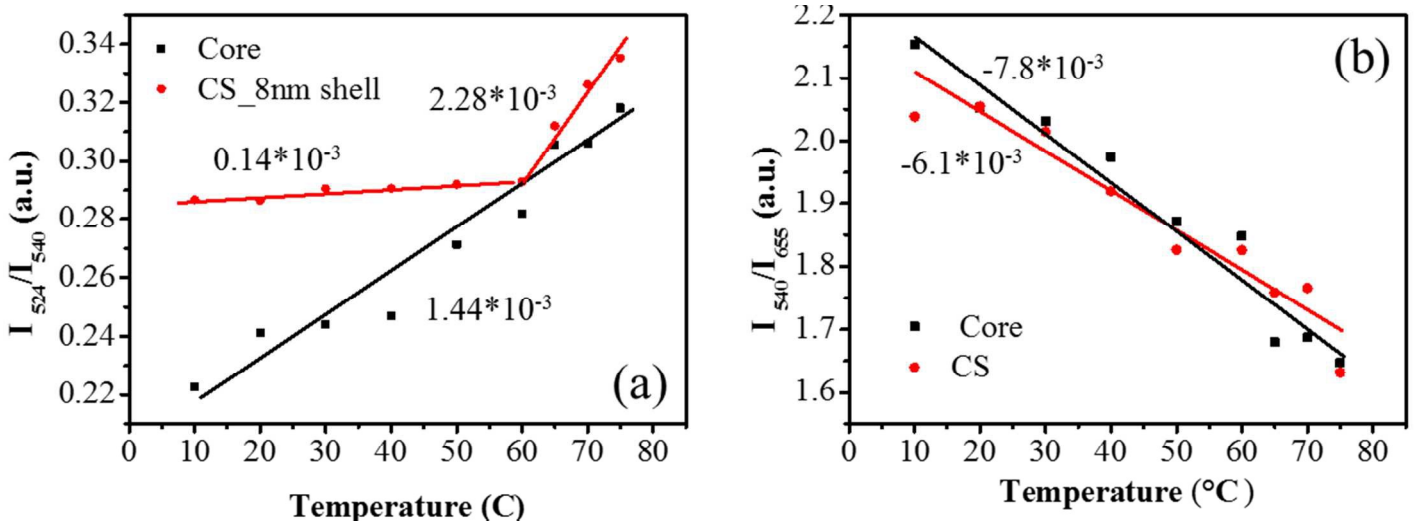

Figure 5 Emission intensity ratio (a) of 524 nm/540 nm from core and core-shell UCNPs and (b) emission intensity ratio of 540 nm/655 nm from core and core-shell UCNPs as a function of temperature.

The ratiometric emissions (I_{524}/I_{540}) from the $NaYF_4:Yb^{3+}$, Er^{3+} UCNPs have been broadly used in nanoscale thermometry[56] because the population distributions on $^2H_{11/2}$ and $^4S_{3/2}$ are dominated by Boltzmann's thermal distribution and elevated temperature leads to rapid population of the $^2H_{11/2}$ state[57]. Figure 5 shows the intensity ratios of 524 nm to 540 nm (I_{524}/I_{540}) and 540 nm to 655 nm (I_{540}/I_{655}) emissions for the core-only and core-shell nanocrystals. The ratio of I_{524}/I_{540} in Figure 5 (a) for the core nanocrystals shows a linear increase with temperature in the range from 10 ˚C to 80 ˚C, which was consistent with previously reported results [57, 58]. The ratio of I_{524}/I_{540} of core-shell nanocrystals is slightly higher than that of core-only nanocrystals at 10 ºC, which suggests the inert shell effectively saved some population on $^2H_{11/2}$ from nonradioactive relax. As increasing the temperature from 10 ˚C to 60 ˚C, the ratio of I_{524}/I_{540} of core-shell nanocrystals slightly increases, however, the ratio increases quickly when the temperature was increased from 60 ˚C to 75 ˚C. This anomalous temperature-dependent phenomenon was also found and reported by other groups for small sized upconversion nanocrystals [59]. The population distribution changes on $^2H_{11/2}$ and $^4S_{3/2}$ could be caused from surface defects and surface molecular quencher (e.g. water molecular vibration) and temperature. Higher temperature helps to increase the population distribution on $^2H_{11/2}$. On the other hand, stronger surface quenchers would decrease the population on $^2H_{11/2}$ than that on $^4S_{3/2}$ because the higher level excited state of $^2H_{11/2}$ could receive more quenching effect [55]. At the elevated temperatures, not only the thermal factor of nanocrystals would become larger but also the surface quenching effect would be stronger. The slow increase rate of I_{524}/I_{540} of core-shell nanocrystals at the low temperature range is due to the competition of the two different effects. Due to the inert shell which effectively blocks the quenching effect at high temperatures, the fast increasing rate of I_{524}/I_{540} can attribute to the

sole thermal factor. This data suggested the core-shell UCNPs may not be sensitive for temperature measurements in the temperature range from 10 ˚C to 60 ˚C.

Figure 5(b) further shows that the ratios of I_{540}/I_{655} emissions for the core and core-shell nanocrystals linearly decreased with temperature between 10 ˚C to 80 ˚C, which was consistent to the results reported by other authors. [57] Higher temperature increases the comparative influence of the non-radiative relaxation channels, from $^4I_{11/2}$ to $^4I_{13/2}$ and from $^4S_{3/2}$, $^2H_{11/2}$ to $^4F_{9/2}$, leading to an increase of the ratio of I_{540}/I_{655} emission.

Conclusion

In summary, we demonstrated here that oleic acid and oleylamine as co-surfactants with a right balance can be used to synthesize homogeneous core-shell $NaYF_4$ nanocrystals. The intact shells with controlled thickness was useful in fully protecting the core nanocrystal from quenching by the surface ligands and solvent. This passivation effect by the intact shells enhanced the luminescent intensities particularly for violet emissions by a factor of up to 30 times. Our key finding reported here is that coating UCNPs with the inert shells improved the luminescent emission stability and reversibility of UCNPs against quenching caused by increased temperature or decreased pH. Moreover, we found that the upconversion emissions at different temperature for both core-only and core-shell UCNPs were fully recoverable but once the UCNPs experienced lower pH conditions (< pH=7) condition their luminescence were observed being permanently quenched suggesting that the acidic environment has chemically damaged the surface of the nanocrystals. Furthermore, by a careful characterization, we found the ratiometric emissions from the core-shell UCNPs were less sensitive to response to the temperature changes in the range from 10 ˚C to 60 ˚C. This work suggests that the luminescence stability and reversibility properties need to be taken into the consideration by optimizing the core-shell designs of upconversion nanocrystals in order to improve many nanoscale bio sensing applications according to the specific requirements by temperature and pH conditions.

Acknowledgements:

We thank D. Birch and Nicole in the Microscope Unit at Macquarie University for their help on TEM characterizations. This project is primarily supported by the Australian Research Council (ARC) Future Fellowship Scheme (FT 130100517; D. Jin), Macquarie University Research Fellowship Scheme (X. Xu) and

China Scholarship Council CSC scholarships (No.201206170136, D. Liu). D. Jin and E. Goldys acknowledge partial support from ARC Centre of Excellence for Nanoscale Biophotonics CE14010003.

Reference

1. B. Zhou, B. Y. Shi, D. Y. Jin and X. G. Liu, *Nat Nanotechnol*, 2015, **10**, 924-936.
2. D. Liu, X. Xu, Y. Du, X. Qin, Y. Zhang, C. Ma, S. Wen, W. Ren, E. M. Goldys, J. A. Piper, S. Dou, X. Liu and D. Jin, *Nat Commun*, 2016, **7**.
3. F. Wang and X. Liu, *J Am Chem Soc*, 2008, **130**, 5642-5643.
4. Y. Lu, J. Zhao, R. Zhang, Y. Liu, D. Liu, E. M. Goldys, X. Yang, P. Xi, A. Sunna and J. Lu, *Nature Photonics*, 2014, **8**, 32-36.
5. J. B. Zhao, Z. D. Lu, Y. D. Yin, C. Mcrae, J. A. Piper, J. M. Dawes, D. Y. Jin and E. M. Goldys, *Nanoscale*, 2013, **5**, 944-952.
6. J. Shen, L. Zhao and G. Han, *Advanced drug delivery reviews*, 2013, **65**, 744-755.
7. S. Wu, G. Han, D. J. Milliron, S. Aloni, V. Altoe, D. V. Talapin, B. E. Cohen and P. J. Schuck, *Proceedings of the National Academy of Sciences*, 2009, **106**, 10917-10921.
8. D. Lu, S. K. Cho, S. Ahn, L. Brun, C. J. Summers and W. Park, *Acs Nano*, 2014, **8**, 7780-7792.
9. A. Gnach, T. Lipinski, A. Bednarkiewicz, J. Rybka and J. A. Capobianco, *Chem Soc Rev*, 2015, **44**, 1561-1584.
10. D. E. Achatz, R. Ali and O. S. Wolfbeis, in *Top Curr Chem*, Springer, 2010, pp. 29-50.
11. D. E. Achatz, R. Ali and O. S. Wolfbeis, *Top Curr Chem*, 2011, **300**, 29-50.
12. Q. Liu, J. J. Peng, L. N. Sun and F. Y. Li, *Acs Nano*, 2011, **5**, 8040-8048.
13. R. Arppe, T. Näreoja, S. Nylund, L. Mattsson, S. Koho, J. M. Rosenholm, T. Soukka and M. Schäferling, *Nanoscale*, 2014, **6**, 6837-6843.
14. K. L. Wong, G. L. Law, Y. Y. Yang and W. T. Wong, *Advanced Materials*, 2006, **18**, 1051-1054.
15. L. Cheng, C. Wang and Z. Liu, *Nanoscale*, 2013, **5**, 23-37.
16. W. Zheng, S. Y. Zhou, Z. Chen, P. Hu, Y. S. Liu, D. T. Tu, H. M. Zhu, R. F. Li, M. D. Huang and X. Y. Chen, *Angew Chem Int Edit*, 2013, **52**, 6671-6676.
17. Q. Liu, W. Feng, T. S. Yang, T. Yi and F. Y. Li, *Nat Protoc*, 2013, **8**, 2033-2044.
18. P. Huang, W. Zheng, S. Zhou, D. Tu, Z. Chen, H. Zhu, R. Li, E. Ma, M. Huang and X. Chen, *Angewandte Chemie International Edition*, 2014, **53**, 1252-1257.
19. Y. Min, J. Li, F. Liu, E. K. Yeow and B. Xing, *Angewandte Chemie International Edition*, 2014, **53**, 1012-1016.
20. Y. Yang, Q. Shao, R. Deng, C. Wang, X. Teng, K. Cheng, Z. Cheng, L. Huang, Z. Liu and X. Liu, *Angewandte Chemie International Edition*, 2012, **51**, 3125-3129.
21. X. Wu, Y. Zhang, K. Takle, O. Bilsel, Z. Li, H. Lee, Z. Zhang, D. Li, W. Fan and C. Duan, *Acs Nano*, 2016.
22. D. M. Yang, P. A. Ma, Z. Y. Hou, Z. Y. Cheng, C. X. Li and J. Lin, *Chem Soc Rev*, 2015, **44**, 1416-1448.
23. Y. M. Yang, *Microchim Acta*, 2014, **181**, 263-294.
24. F. Vetrone, R. Naccache, A. Zamarron, A. Juarranz de la Fuente, F. Sanz-Rodríguez, L. Martinez Maestro, E. Martín Rodriguez, D. Jaque, J. García Solé and J. A. Capobianco, *Acs Nano*, 2010, **4**, 3254-3258.
25. R. J. Meier, J. M. Simbürger, T. Soukka and M. Schäferling, *Analytical chemistry*, 2014, **86**, 5535-5540.
26. Y. L. Dai, P. A. Ma, Z. Y. Cheng, X. J. Kang, X. Zhang, Z. Y. Hou, C. X. Li, D. M. Yang, X. F. Zhai and J. Lin, *Acs Nano*, 2012, **6**, 3327-3338.
27. Z. Y. Hou, C. X. Li, P. A. Ma, Z. Y. Cheng, X. J. Li, X. Zhang, Y. L. Dai, D. M. Yang, H. Z. Lian and J. Lin, *Adv Funct Mater*,

2012, **22**, 2713-2722.
28. X. Zhang, P. P. Yang, Y. L. Dai, P. A. Ma, X. J. Li, Z. Y. Cheng, Z. Y. Hou, X. J. Kang, C. X. Li and J. Lin, *Adv Funct Mater*, 2013, **23**, 4067-4078.
29. Y. L. Dai, D. M. Yang, P. A. Ma, X. J. Kang, X. Zhang, C. X. Li, Z. Y. Hou, Z. Y. Cheng and J. Lin, *Biomaterials*, 2012, **33**, 8704-8713.
30. P. Zhao, J. Zhang, Y. H. Zhu, X. L. Yang, X. Jiang, Y. Yuan, C. S. Liu and C. Z. Li, *J Mater Chem B*, 2014, **2**, 8372-8377.
31. Y. Zhang, L. Huang, Z. Li, G. Ma, Y. Zhou and G. Han, *Acs Nano*, 2016.
32. N. Bogdan, F. Vetrone, G. A. Ozin and J. A. Capobianco, *Nano Lett*, 2011, **11**, 835-840.
33. W. F. Xingjun Zhu, Jian Chang, Yan-Wen Tan, Jiachang Li, Min Chen, Yun Sun & Fuyou Li, *Nat Commun*, 2016, **7**, 10.
34. Y. Dai, P. a. Ma, Z. Cheng, X. Kang, X. Zhang, Z. Hou, C. Li, D. Yang, X. Zhai and J. Lin, *Acs Nano*, 2012, **6**, 3327-3338.
35. E. E. Lees, T.-L. Nguyen, A. H. Clayton and P. Mulvaney, *Acs Nano*, 2009, **3**, 1121-1128.
36. S. Wang, J. Feng, S. Song and H. Zhang, *CrystEngComm*, 2013, **15**, 7142-7151.
37. P. Sharma, S. Brown, G. Walter, S. Santra and B. Moudgil, *Adv Colloid Interfac*, 2006, **123**, 471-485.
38. Y. C. Wei, Q. Chen, B. Y. Wu, A. G. Zhou and D. Xing, *Nanoscale*, 2012, **4**, 3901-3909.
39. D. D. Li, Q. Y. Shao, Y. Dong and J. Q. Jiang, *Mater Lett*, 2013, **110**, 233-236.
40. D. Li, Q. Shao, Y. Dong and J. Jiang, *The Journal of Physical Chemistry C*, 2014, **118**, 22807-22813.
41. B. Zhou, B. Shi, D. Jin and X. Liu, *Nature nanotechnology*, 2015, **10**, 924-936.
42. J. C. Boyer and F. C. J. M. van Veggel, *Nanoscale*, 2010, **2**, 1417-1419.
43. D. Q. Chen and P. Huang, *Dalton T*, 2014, **43**, 11299-11304.
44. Y. F. Wang, L. D. Sun, J. W. Xiao, W. Feng, J. C. Zhou, J. Shen and C. H. Yan, *Chem-Eur J*, 2012, **18**, 5558-5564.
45. N. Bogdan, E. M. Rodríguez, F. Sanz-Rodríguez, M. C. I. de la Cruz, Á. Juarranz, D. Jaque, J. G. Solé and J. A. Capobianco, *Nanoscale*, 2012, **4**, 3647-3650.
46. N. J. J. Johnson, A. Korinek, C. H. Dong and F. C. J. M. van Veggel, *J Am Chem Soc*, 2012, **134**, 11068-11071.
47. L. X. Zhang, A. Mckay and D. Y. Jin, *Rsc Adv*, 2013, **3**, 8670-8673.
48. N. J. Johnson and F. C. van Veggel, *Nano Research*, 2013, **6**, 547-561.
49. L. P. Qian, D. Yuan, G. S. Yi and G. M. Chow, *J Mater Res*, 2009, **24**, 3559-3568.
50. Q. Tian, K. Tao and K. Sun, *Micro Nano Lett*, 2013, **8**, 731-734.
51. L. X. Liu, F. Qin, H. Zhao, T. Q. Lv, Z. G. Zhang and W. W. Cao, *Opt Lett*, 2013, **38**, 2101-2103.
52. J. Shen, G. Y. Chen, T. Y. Ohulchanskyy, S. J. Kesseli, S. Buchholz, Z. P. Li, P. N. Prasad and G. Han, *Small*, 2013, **9**, 3213-3217.
53. S. Zhou, W. Zheng, Z. Chen, D. Tu, Y. Liu, E. Ma, R. Li, H. Zhu, M. Huang and X. Chen, *Angewandte Chemie*, 2014, **126**, 12706-12710.
54. J. Xu, S. Zhou, D. Tu, W. Zheng, P. Huang, R. Li, Z. Chen, M. Huang and X. Chen, *Chemical Science*, 2016, **7**, 2572-2578.
55. F. Wang, J. Wang and X. Liu, *Angewandte Chemie*, 2010, **122**, 7618-7622.
56. L. H. Fischer, G. S. Harms and O. S. Wolfbeis, *Angewandte Chemie International Edition*, 2011, **50**, 4546-4551.
57. W. Yu, W. Xu, H. Song and S. Zhang, *Dalton T*, 2014, **43**, 6139-6147.
58. Y. Tian, B. Tian, P. Huang, L. Wang and B. Chen, *Rsc Adv*, 2015, **5**, 14123-14128.
59. J. Xi, M. Ding, J. Dai, Y. Pan, D. Chen and Z. Ji, *Journal of Materials Science: Materials in Electronics*, 1-17.

We report the emission stability and reversibility of $NaYF_4:Yb^{3+},Er^{3+}$ core and core-shell nanocrystals at different temperatures and pH values.